Pergamon

Int. J. Solids Structures Vol. 34, No. 6, pp. 685–702, 1997

0020–7683/97 $17.00 + .00

PII: S0020–7683(96)00047–9

EXACT PIEZOELASTIC SOLUTION OF SIMPLY-SUPPORTED ORTHOTROPIC CIRCULAR CYLINDRICAL PANEL IN CYLINDRICAL BENDING

P. C. DUMIR, G. P. DUBE and SANTOSH KAPURIA
Applied Mechanics Department, I.I.T. Delhi, New Delhi-110016, India

(*Received* 1 *August* 1995; *in revised form* 19 *March* 1996)

Abstract—This work presents an exact piezoelastic solution of an infinitely long, simply-supported, orthotropic, piezoelectric, radially polarised, circular cylindrical shell panel in cylindrical bending under pressure and electrostatic excitation. The general solution of the governing differential equations is obtained by separation of variables. The displacements and electric potential are expanded in appropriate trigonometric Fourier series in the circumferential coordinate to satisfy the boundary conditions at the simply-supported longitudinal edges. The governing equations reduce to Euler–Cauchy type of ordinary differential equations. Their general solution involves six constants for each Fourier component. These are solved from the algebraic equations obtained by satisfying the boundary conditions at the lateral surfaces. The solution of the inverse problem of inferring the applied pressure field from the given measured distribution of electrical potential difference between the lateral surfaces of the shell has also been presented. Numerical results are presented for typical pressure and electrostatic loadings for various values of radius to thickness ratio. Copyright © 1997 Elsevier Science Ltd.

1. INTRODUCTION

The coupling effect existing between the elastic and electric fields in piezoelectric materials is used in various engineering applications. The direct piezoeffect is used in sensors in electromechanical transducers to infer the deformation from the induced electrical potential difference. The converse piezoeffect is used in electromechanical actuators for controlling an entity by the application of appropriate electrical potential differences. The piezoelectric materials have immense potential for use as distributed actuators and sensors for *active* control of *smart* structural systems (Crawley, 1994). Very few exact solutions of the three dimensional field equations are available for the coupled response of piezoelectric elements to electromechanical loading. These analytical solutions are needed to assess the accuracy of the various two dimensional plate and shell theory formulations. Ray *et al.* (1992, 1993a) presented exact solutions for static analyses of a simply-supported piezoelectric flat panel and a layered *intelligent* flat panel under cylindrical bending. Three dimensional exact analyses of simply-supported rectangular plate coupled with distributed sensors and actuators have been presented by Ray *et al.* (1993b) and Heyliger (1994). Mitchell and Reddy (1995) have presented a power series solution for static analysis of an axisymmetric problem of axial loading on a composite cylinder with surfacebonded or embedded piezoelectric laminae. Ren (1987) has presented the exact elasticity solution of simply-supported laminated circular cylindrical panels in cylindrical bending.

In this work we present an exact piezoelastic solution of an infinitely long, simply-supported, orthotropic, piezoelectric, radially polarised, circular cylindrical shell panel in cylindrical bending under pressure and electrostatic excitation. The general solution of the governing differential equations is obtained by separation of variables. The displacements and electric potential are expanded in the appropriate trigonometric Fourier series in the circumferential coordinate to satisfy the boundary conditions at the simply-supported longitudinal ends. The prescribed electromechanical functions on the lateral boundary are expanded in terms of the trigonometric Fourier series in the circumferential coordinate. The governing equations reduce to Euler–Cauchy type of ordinary differential equations.

Their general solution involves six constants for each Fourier component. The boundary conditions at the lateral surfaces for each Fourier component yield these constants. The inverse problem of inferring the applied pressure field from the given measured distribution of electrical potential difference between the lateral surfaces of the shell has also been solved. Since the electroelasticity field equations are used, the exact solution presented is valid for both thin and thick shells as well as for deep and shallow shells. Numerical results are presented for typical pressure and electrostatic loadings for various values of radius to thickness ratio.

2. GOVERNING EQUATIONS

The linear constitutive equations of a piezoelectric medium are given by

$$\{\sigma\} = [C]\{\varepsilon\} - [e]^{\mathrm{T}}\{E\}, \quad \{D\} = [e]\{\varepsilon\} + [\eta]\{E\}, \tag{1}$$

where the stress components $\{\sigma\}$, the strain components $\{\varepsilon\}$, the electric field vector $\{E\}$ and the electric displacement vector $\{D\}$ are given in cylindrical coordinate system (r, θ, z), by:

$$\{\sigma\} = [\sigma_r \quad \sigma_\theta \quad \sigma_z \quad \tau_{\theta z} \quad \tau_{zr} \quad \tau_{r\theta}]^{\mathrm{T}}, \quad \{E\} = [E_r \quad E_\theta \quad E_z]^{\mathrm{T}}$$
$$\{\varepsilon\} = [\varepsilon_r \quad \varepsilon_\theta \quad \varepsilon_z \quad \gamma_{\theta z} \quad \gamma_{zr} \quad \gamma_{r\theta}]^{\mathrm{T}}, \quad \{D\} = [D_r \quad D_\theta \quad D_z]^{\mathrm{T}}$$

$[C]$, $[e]$ and $[\eta]$ denote, respectively, the matrices of elastic constants, piezoelectric constants and dielectric constants of the piezoelastic material. The equations of equilibrium in the absence of body force and the charge equation of equilibrium of electrostatics in cylindrical coordinates are

$$\begin{aligned} \sigma_{r,r} + \tau_{r\theta,\theta}/r + \tau_{zr,z} + (\sigma_r - \sigma_\theta)/r &= 0 \\ \tau_{r\theta,r} + \sigma_{\theta,\theta}/r + \tau_{\theta z,z} + 2\tau_{r\theta}/r &= 0 \\ \tau_{zr,r} + \tau_{\theta z,\theta}/r + \sigma_{z,z} + \tau_{zr}/r &= 0 \\ D_{r,r} + D_r/r + D_{\theta,\theta}/r + D_{z,z} &= 0 \end{aligned} \tag{2}$$

where differentiation is denoted by a subscript comma. We consider a cylindrically orthotropic piezoelectric material with poling in the radial direction. The matrices $[C]$, $[e]$ and $[\eta]$, as given by Tiersten (1969), are

$$[C] = \begin{bmatrix} C_{11} & C_{12} & C_{13} & 0 & 0 & 0 \\ C_{12} & C_{22} & C_{23} & 0 & 0 & 0 \\ C_{13} & C_{23} & C_{33} & 0 & 0 & 0 \\ 0 & 0 & 0 & C_{44} & 0 & 0 \\ 0 & 0 & 0 & 0 & C_{55} & 0 \\ 0 & 0 & 0 & 0 & 0 & C_{66} \end{bmatrix}$$

$$[e] = \begin{bmatrix} e_1 & e_2 & e_3 & 0 & 0 & 0 \\ 0 & 0 & 0 & 0 & 0 & e_6 \\ 0 & 0 & 0 & 0 & e_5 & 0 \end{bmatrix} \quad [\eta] = \begin{bmatrix} \eta_1 & 0 & 0 \\ 0 & \eta_2 & 0 \\ 0 & 0 & \eta_3 \end{bmatrix}. \tag{3}$$

Consider an infinitely long circular cylindrical shell panel of mean radius R, thickness h,

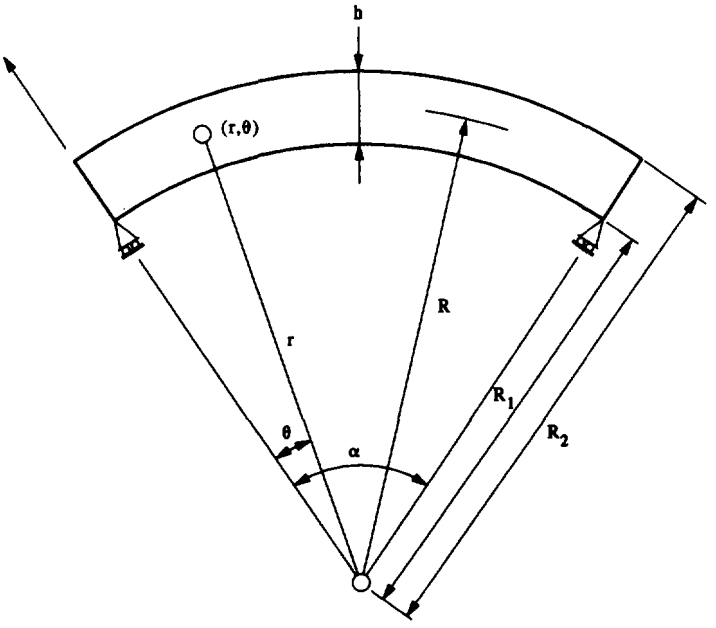

Fig. 1. Geometry of panel.

and angular span α as shown in Fig. 1. Its longitudinal ends at $\theta = 0, \alpha$ are simply-supported and electrically grounded. Its lateral surfaces at $r = R_1 = R - h/2$ and at $r = R_2 = R + h/2$ are subjected to electrical and traction boundary conditions which do not vary along the axial coordinate z. The geometry, material property and boundary conditions of such a panel ensure a state of plane strain with axial displacement zero and all displacements, strains, stresses, electrical potential, electrical field and electrical displacement vector being invariant in the z direction. The piezoelastic problem is thus a two-dimensional one in radial and circumferential coordinates.

The strains are related to the radial and circumferential displacement components u and v by

$$\varepsilon_r = u_{,r}, \quad \varepsilon_\theta = (u + v_{,\theta})/r, \quad \gamma_{r\theta} = (u_{,\theta} - v)/r + v_{,r}, \quad \varepsilon_z = \gamma_{zr} = \gamma_{z\theta} = 0. \tag{4}$$

The electric field is related to the electric potential, ϕ, of the piezoelectric medium by

$$E_r = -\phi_{,r}, \quad E_\theta = -\phi_{,\theta}/r, \quad E_z = -\phi_{,z}. \tag{5}$$

Using expressions (3)–(5), the constitutive eqns (1) can be written as

$$\begin{aligned} \sigma_r &= C_{11}u_{,r} + C_{12}(u + v_{,\theta})/r + e_1\phi_{,r} \\ \sigma_\theta &= C_{12}u_{,r} + C_{22}(u + v_{,\theta})/r + e_2\phi_{,r} \\ \sigma_z &= C_{13}u_{,r} + C_{23}(u + v_{,\theta})/r + e_3\phi_{,r} \end{aligned} \tag{6}$$

$$\tau_{\theta z} = \tau_{zr} = 0, \quad \tau_{r\theta} = C_{66}[(u_{,\theta} - v)/r + v_{,r}] + e_6\phi_{,\theta}/r$$

$$D_r = e_1u_{,r} + e_2(u + v_{,\theta})/r - \eta_1\phi_{,r}, \quad D_\theta = e_6[(u_{,\theta} - v)/r + v_{,r}] - \eta_2\phi_{,\theta}/r, \quad D_z = 0. \tag{7}$$

Let the prescribed pressure and electrical potential or electric displacement D_r to cause actuation strain at the inner and outer surfaces be $q_1(\theta)$, $\phi_1(\theta)$ or $D_1(\theta)$ and $q_2(\theta)$, $\phi_2(\theta)$ or $D_2(\theta)$, respectively. Boundary conditions at the longitudinal ends at $\theta = 0, \alpha$ are:

$$u = 0, \quad \sigma_\theta = 0, \quad \phi = 0. \tag{8}$$

Boundary conditions at the lateral surfaces at $r = R_1, R_2$ are :

$$\begin{aligned}
&\sigma_r(R_1,\theta) = -q_1(\theta), \quad \tau_{r\theta}(R_1,\theta) = 0, \quad \phi(R_1,\theta) = \phi_1(\theta) \quad \text{or } D_r(R_1,\theta) = D_1(\theta)\\
&\sigma_r(R_2,\theta) = -q_2(\theta), \quad \tau_{r\theta}(R_2,\theta) = 0, \quad \phi(R_2,\theta) = \phi_2(\theta) \quad \text{or } D_r(R_2,\theta) = D_2(\theta).
\end{aligned} \tag{9}$$

We express all the governing equations in terms of the following dimensionless entities :

$$\begin{aligned}
&u_i^* = u_i/h, && \sigma_{ij}^* = \sigma_{ij}R/hY_r, && \phi^* = \phi|d_1|/h, && R_i^* = R_i/R,\\
&D_i^* = D_iR/h|d_1|Y_r, && E_i^* = E_iR|d_1|/h, && C_{ij}^* = C_{ij}/Y_r, && r^* = r/R,\\
&e_i^* = e_i/|d_1|Y_r, && \eta_i^* = \eta_i/|d_1|^2Y_r, && \varepsilon_{ij}^* = \varepsilon_{ij}R/h, && z^* = z/R,
\end{aligned} \tag{10}$$

where Y_r and d_1 denote respectively the Young's modulus and the piezoelectric coefficient in the radial direction. For simplicity, in the sequel, we drop the superscript * from the dimensionless entities. The dimensionless form of eqns (1)–(9) is exactly the same as given earlier.

3. GENERAL SOLUTION OF GOVERNING EQUATIONS

The solution of the boundary value problem, satisfying the boundary conditions (8), is taken in the following separable form :

$$(u,\phi) = \sum_{n=1}^{\infty} (u_n,\phi_n)\sin s_n\theta, \quad v = \sum_{n=1}^{\infty} v_n\cos s_n\theta; \quad s_n = n\pi/\alpha. \tag{11}$$

Substitution of u, v and ϕ from eqn (11) into (6) and (7) yields

$$\begin{aligned}
\sigma_r &= \sum_{n=1}^{\infty} [C_{11}u_n' + C_{12}(u_n - s_nv_n)/r + e_1\phi_n']\sin s_n\theta,\\
\sigma_\theta &= \sum_{n=1}^{\infty} [C_{12}u_n' + C_{22}(u_n - s_nv_n)/r + e_2\phi_n']\sin s_n\theta,\\
\sigma_z &= \sum_{n=1}^{\infty} [C_{13}u_n' + C_{23}(u_n - s_nv_n)/r + e_3\phi_n']\sin s_n\theta,\\
\tau_{r\theta} &= \sum_{n=1}^{\infty} [C_{66}\{(s_nu_n - v_n)/r + v_n'\} + s_ne_6\phi_n/r]\cos s_n\theta,\\
\tau_{\theta z} &= \tau_{zr} = D_z = 0,\\
D_r &= \sum_{n=1}^{\infty} [e_1u_n' + e_2(u_n - s_nv_n)/r - \eta_1\phi_n']\sin s_n\theta,\\
D_\theta &= \sum_{n=1}^{\infty} [e_6\{(s_nu_n - v_n)/r + v_n'\} - s_n\eta_2\phi_n/r]\cos s_n\theta
\end{aligned} \tag{12}$$

where $()' = \partial()/\partial r^*$. In order to satisfy the boundary conditions (9) on the lateral surfaces, we expand the functions $q_i(\theta)$, $\phi_i(\theta)$, $D_i(\theta)$ in Fourier series :

$$q_i(\theta) = \sum_{n=1}^{\infty} q_i^n \sin s_n\theta, \quad \phi_i(\theta) = \sum_{n=1}^{\infty} \phi_i^n \sin s_n\theta, \quad D_i(\theta) = \sum_{n=1}^{\infty} D_i^n \sin s_n\theta, \tag{13}$$

where

$$f_i^n = \frac{2}{\alpha}\int_0^{\alpha} f_i(\theta)\sin s_n\theta\,\mathrm{d}\theta.$$

Substitution of σ_{ij} and D_i from (12) into the equations of equilibrium (2) yield

$$C_{11}(u_n''+u_n'/r)-(C_{66}s_n^2+C_{22})u_n/r^2-s_n(C_{12}+C_{66})v_n'/r$$
$$+s_n(C_{66}+C_{22})v_n/r^2+e_1\phi_n''+(e_1-e_2)\phi_n'/r-s_n^2e_6\phi_n/r^2=0, \quad (14a)$$

$$s_n(C_{12}+C_{66})u_n'/r+(C_{66}+C_{22})s_nu_n/r^2+C_{66}(v_n''+v_n'/r)$$
$$-(C_{66}+s_n^2C_{22})v_n/r^2+(e_6+e_2)s_n\phi_n'/r+s_ne_6\phi_n/r^2=0, \quad (14b)$$

$$e_1u_n''+(e_1+e_2)u_n'/r-s_n^2e_6u_n/r^2-(e_2+e_6)s_nv_n'/r$$
$$+s_ne_6v_n/r^2-\eta_1(\phi_n''+\phi_n'/r)+s_n^2\eta_2\phi_n/r^2=0. \quad (14c)$$

Equations (14) are Euler–Cauchy type of coupled homogeneous ordinary differential equations for u_n, v_n and ϕ_n. The solution of (14) is of the following form:

$$U_n=[u_n \quad v_n \quad \phi_n]^{\mathrm{T}}=fr^{\lambda} \quad \text{with } f^{\mathrm{T}}=[f_1 \quad f_2 \quad f_3]. \quad (15)$$

Substitution of solution (15) into eqns (14) yields the following homogeneous linear algebraic equations:

$$A(\lambda)f=0. \quad (16)$$

The elements of matrix A are

$$a_{11}=C_{11}\lambda^2-(C_{22}+C_{66}s_n^2) \quad a_{12}=s_n[C_{66}+C_{22}-\lambda(C_{12}+C_{66})] \quad a_{13}=\lambda^2e_1-\lambda e_2-s_n^2e_6$$
$$a_{21}=s_n[C_{22}+C_{66}+\lambda(C_{12}+C_{66})] \quad a_{22}=\lambda^2C_{66}-(C_{66}+s_n^2C_{22}) \quad a_{23}=s_n[e_6+\lambda(e_2+e_6)]$$
$$a_{31}=e_1\lambda^2+e_2\lambda-s_n^2e_6 \quad a_{32}=s_n[e_6-(e_2+e_6)\lambda] \quad a_{33}=-\eta_1\lambda^2+\eta_2s_n^2. \quad (17)$$

The characteristic equation of (16) is given by

$$|A(\lambda)|=-a\lambda^6+b\lambda^4+c\lambda^2+d=0 \quad (18)$$

where

$$a=C_{66}(e_1^2+\eta_1C_{11}) \quad d=C_{22}(e_6^2+\eta_2C_{66})s_n^2(s_n^2-1)^2$$
$$b=s_n^2[\eta_1(C_{11}C_{22}-C_{12}^2-2C_{12}C_{66})+\eta_2C_{11}C_{66}+C_{11}(e_2+e_6)^2$$
$$-2e_1e_2(C_{12}+C_{66})-2C_{12}e_1e_6+e_1^2C_{22}]+C_{66}[(C_{11}+C_{22})\eta_1+e_1^2+e_2^2]$$
$$c=-C_{66}(C_{22}\eta_1+e_2^2)(s_n^2-1)^2+2s_n^2(s_n^2-1)e_6(C_{12}e_2-C_{22}e_1)$$
$$-s_n^2(C_{11}+C_{22})(e_6^2+\eta_2C_{66})+s_n^4[\eta_2(C_{12}^2+2C_{12}C_{66}-C_{11}C_{22})+2C_{12}e_6^2]. \quad (19)$$

The characteristic eqn (18) can be transformed into

$$\Lambda^3+D\Lambda+F=0 \quad (20)$$

where

$$\Lambda = \lambda^2 - b/3a, \quad D = -(b^2+3ca)/3a^2, \quad F = -(2b^3+9abc+27da^2)/27a^3. \tag{21}$$

The nature of the roots of eqn (20) depends on the sign of $G = F^2/4 + D^3/27$ (Smirnov, 1964):

1. If $G > 0$, then one root is real and the other two are complex conjugate as follows:

$$\Lambda_1 = \omega - \rho, \quad \Lambda_2, \Lambda_3 = -\Lambda_1/2 \pm i\sqrt{3}(\omega+\rho)/2,$$
$$\text{with } \omega = (\sqrt{G} - F/2)^{1/3}, \quad \rho = (\sqrt{G} + F/2)^{1/3}. \tag{22}$$

2. If $G \leqslant 0$, then the roots are real. If $G < 0$, then the roots are distinct; if $G = 0$ and $D \neq 0$, then one root is a double root. The roots are given by

$$\Lambda_j = 2(-D/3)^{1/2} \cos[\{\gamma + 2\pi(j-1)\}/3], \quad j = 1, 2, 3, \quad \text{where} \quad \cos\gamma = -\sqrt{27}F/2(-D)^{3/2}. \tag{23}$$

If $G = 0$ and $D = 0$, then all the three real roots are equal: $\Lambda_j = 0$.

The general solution of eqn (14) is the sum of the six solutions for the six roots λ of eqn (18). For a pair of complex conjugate roots $\lambda^2 = \Lambda_j + b/3a = \alpha_j \pm i\beta_j$, the four roots of eqn (18) are

$$\lambda = \pm(\alpha \pm i\beta) \quad \text{where } (\alpha, \beta) = (\alpha_j^2 + \beta_j^2)^{1/4}(\cos\delta, \sin\delta) \quad \text{with } \delta = \tan^{-1}(\beta_j/\alpha_j)/2. \tag{24}$$

The solution of eqn (14) for $\lambda = \alpha \pm i\beta$, in terms of arbitrary constants C_1 and C_2, is

$$U_n = [\Re(g) r^\alpha \sin(\beta \ln r) + \Im(g) r^\alpha \cos(\beta \ln r)]C_1 + [\Re(g) r^\alpha \cos(\beta \ln r) - \Im(g) r^\alpha \sin(\beta \ln r)]C_2 \tag{25a}$$

where

$$g = [A_{k1} \quad A_{k2} \quad A_{k3}]^{\mathrm{T}}/l, \quad l = [A_{k1}\bar{A}_{k1} + A_{k2}\bar{A}_{k2} + A_{k3}\bar{A}_{k3}]^{1/2}. \tag{25b}$$

A_{ij} are the cofactors of matrix A for $\lambda = \alpha + i\beta$, $\bar{z}$ is the complex conjugate of z, k is any row index for which $l \neq 0$. $\Re$ and $\Im$ indicate the real and imaginary parts of a complex number.

For a distinct real root Λ_j, $\lambda = \pm(\Lambda_j + b/3a)^{1/2}$ can be real or imaginary. If $\Lambda_j + b/3a < 0$, then $\lambda = \pm ip$ with $p = |\Lambda_j + b/3a|^{1/2}$. The solution of eqn (14) for $\lambda = \pm ip$ is given by eqn (25) with $\alpha = 0$ and $\beta = p$. If $\Lambda_j + b/3a > 0$, then $\lambda = \pm p$. The solution for $\lambda = p$ in terms of an arbitrary constant C_3 is

$$U_n = g r^p C_3 \tag{26}$$

where g is given by eqn (25) with cofactors of matrix A evaluated for $\lambda = p$. The solution for $\lambda = -p$ is similar. The solutions for multiple roots of (20) are not listed since such roots do not arise for any s_n for the materials considered in this study.

Thus the general solution of eqns (14) is

$$u_n = \sum_{j=1}^{6} F_{1j}^n(r) C_j, \quad v_n = \sum_{j=1}^{6} F_{2j}^n(r) C_j, \quad \phi_n = \sum_{j=1}^{6} F_{3j}^n(r) C_j. \tag{27}$$

Depending on the nature of the six roots λ of eqn (18), $F_{ij}^n(r)$, $i = 1, 2, 3$, have appropriate functional form given in eqns (25a) and (26). For a real root $\lambda_3 = p$:

$$F^n_{i3} = A_{ki}(p)r^p/l, \quad \Rightarrow F^{n'}_{i3} = A_{ki}(p)pr^{p-1}/l \tag{28}$$

and for a pair of complex conjugate roots $\lambda_1, \lambda_2 = \alpha \pm i\beta$:

$$[F^n_{11} \quad F^n_{21} \quad F^n_{31}]^T = [\Re(g)r^\alpha \sin(\beta \ln r) + \Im(g)r^\alpha \cos(\beta \ln r)] \tag{29a}$$

$$[F^n_{12} \quad F^n_{22} \quad F^n_{32}]^T = [\Re(g)r^\alpha \cos(\beta \ln r) - \Im(g)r^\alpha \sin(\beta \ln r)] \tag{29b}$$

$$[F^{n'}_{11} \quad F^{n'}_{21} \quad F^{n'}_{31}]^T = [\{\alpha\Re(g) - \beta\Im(g)\}r^{\alpha-1} \sin(\beta \ln r) + [\{\alpha\Im(g) + \beta\Re(g)\}r^{\alpha-1} \cos(\beta \ln r)] \tag{30a}$$

$$[F^{n'}_{12} \quad F^{n'}_{22} \quad F^{n'}_{32}]^T = [\{\alpha\Re(g) - \beta\Im(g)\}r^{\alpha-1} \cos(\beta \ln r) - [\{\alpha\Im(g) + \beta\Re(g)\}r^{\alpha-1} \sin(\beta \ln r)]. \tag{30b}$$

Substituting u_n, v_n, ϕ_n from eqn (27) into eqn (12) yields the following expressions of the nth Fourier component of stress, electric displacement and electric field components:

$$\sigma^n_r(r) = \sum_{j=1}^{6} [C_{11}F^{n'}_{1j} + C_{12}(F^n_{1j} - s_nF^n_{2j})/r + e_1F^{n'}_{3j}]C_j, \tag{31}$$

$$\sigma^n_\theta(r) = \sum_{j=1}^{6} [C_{12}F^{n'}_{1j} + C_{22}(F^n_{1j} - s_nF^n_{2j})/r + e_2F^{n'}_{3j}]C_j, \tag{32}$$

$$\sigma^n_z(r) = \sum_{j=1}^{6} [C_{13}F^{n'}_{1j} + C_{23}(F^n_{1j} - s_nF^n_{2j})/r + e_3F^{n'}_{3j}]C_j, \tag{33}$$

$$\tau^n_{r\theta}(r) = \sum_{j=1}^{6} [C_{66}\{(s_nF^n_{1j} - F^n_{2j})/r + F^{n'}_{2j}\} + s_ne_6F^n_{3j}/r]C_j, \tag{34}$$

$$D^n_r(r) = \sum_{j=1}^{6} [e_1F^{n'}_{1j} + e_2(F^n_{1j} - s_nF^n_{2j})/r - \eta_1F^{n'}_{3j}]C_j, \tag{35}$$

$$D^n_\theta(r) = \sum_{j=1}^{6} [e_6\{(s_nF^n_{1j} - F^n_{2j})/r + F^{n'}_{2j}\} - s_n\eta_2F^n_{3j}/r]C_j, \tag{36}$$

$$E^n_r(r) = \sum_{j=1}^{6} [-F^{n'}_{3j}]C_j, \quad E^n_\theta(r) = \sum_{j=1}^{6} [-s_nF^n_{3j}/r]C_j. \tag{37}$$

4. SOLUTION OF DIRECT PROBLEM

The solution of the direct problem is obtained by substitution of expressions (31), (34), (27), and (35) for σ^n_r, $\tau^n_{r\theta}$ and ϕ_n or D^n_r and the expansions (13) into the six electromechanical boundary conditions (9). This yields six linear algebraic equations for $C^n = [C_1 \quad C_2 \quad C_3 \quad C_4 \quad C_5 \quad C_6]^T$:

$$K^nC^n = F^n \tag{38}$$

where, for $i = 1, 2$:

$$k_{ij}^n = [C_{11}F_{1j}^{n'} + C_{12}(F_{1j}^n - s_n F_{2j}^n)/r + e_1 F_{3j}^{n'}]|_{r=R_i}, \quad F_i^n = -q_i^n,$$

$$k_{2+i,j}^n = [C_{66}\{(s_n F_{1j}^n - F_{2j}^n)/r + F_{2j}^{n'}\} + s_n e_6 F_{3j}^n/r]|_{r=R_i}, \quad F_{2+i}^n = 0. \tag{39}$$

If ϕ is prescribed then:

$$k_{4+i,j}^n = F_{3j}^n(R_i), \quad F_{4+i}^n = \phi_i^n. \tag{40}$$

Else, if D_r is prescribed then:

$$k_{4+i,j}^n = [e_1 F_{1j}^{n'} + e_2(F_{1j}^n - s_n F_{2j}^n)/r - \eta_1 F_{3j}^{n'}]|_{r=R_i}, \quad F_{4+i}^n = D_i^n. \tag{41}$$

The arbitrary constants C_j for the given boundary conditions can be determined for each n from eqn (38). The displacements, electrical potential, stress, electric displacement and electric field components can then be computed using relations (27) and (31)–(37) by taking a finite number of terms, say N, in the series. A convergence study will determine the appropriate value of N to be used for given electromechanical load.

5. SOLUTION OF INVERSE PIEZOELASTIC PROBLEM

Consider an inverse piezoelastic problem in which the cylindrical panel has a known pressure $q_1(\theta)$ inside and is subjected to an unknown pressure profile at the outer surface. This pressure profile $q_2(\theta)$ is to be determined from the known measured potential difference $V(\theta)$ between the outer and inner surfaces. The boundary conditions (9) for the inverse problem have prescribed charge distribution $D_i(\theta)$ and involve the unknown pressure $q_2(\theta)$ which can be determined using the additional condition of potential difference:

$$\phi(R_2, \theta) - \phi(R_1, \theta) = V(\theta) = \sum_{n=1}^{\infty} V^n \sin s_n\theta \quad \text{with } V^n = \frac{2}{\alpha}\int_0^{\alpha} V(\theta) \sin s_n\theta \, d\theta. \tag{42}$$

Using eqn (27), it yields

$$\sum_{j=1}^{6} [F_{3j}^n(R_2) - F_{3j}^n(R_1)]C_j = V^n. \tag{43}$$

Substitution of the expressions (31), (34) and (35) for σ_r^n, $\tau_{r\theta}^n$ and D_r^n, and the expansions (13) into the six electroelastic boundary conditions (9) and the potential difference condition (43) yield the following relations for $C^{n'} = [C_1 \quad C_2 \quad C_3 \quad C_4 \quad C_5 \quad C_6 \quad q_2^n]^T$:

$$K^{n'}C^{n'} = F^{n'} \tag{44}$$

where

$$k_{mj}^{n'} = k_{mj}^n \quad \text{for } m = 1, \ldots, 6, \quad j = 1, \ldots, 6; \quad k_{i7}^{n'} = 0 \quad \text{for } i \neq 2, \quad k_{27}^{n'} = 1$$

$$k_{rj}^{n'} = F_{3j}^{n'}(R_2) - F_{3j}^{n'}(R_1), \quad k_{77}^{n'} = 0, \quad F_7^{n'} = V_n,$$

$$F_j^{n'} = F_j^n, \quad \text{for } j = 1, 3, 4, 5, 6, \quad F_2^{n'} = 0. \tag{45}$$

The unknown constants C_j and the Fourier coefficients q_2^n of the unknown pressure $q_2(\theta)$ are determined by solving the set of seven simultaneous algebraic equations for each value of n. The unknown pressure distribution on the outer surface can then be determined from eqn (13) as $q_2(\theta) = \Sigma_{n=1}^{\infty} q_2^n \sin s_n\theta$.

6. NUMERICAL RESULTS

Results are presented for cylindrical panels subjected to four cases of electromechanical loads:

1. $\phi_1(\theta) = \phi_2(\theta) = 0$, $q_1(\theta) = 0$, $q_2(\theta) = q_0 \sin(\pi\theta/\alpha)$.
2. $\phi_1(\theta) = 0$, $\phi_2(\theta) = -\phi_0 \sin(\pi\theta/\alpha)$, $q_1(\theta) = q_2(\theta) = 0$.
3. $\phi_1(\theta) = \phi_2(\theta) = 0$, $q_1(\theta) = 0$, $q_2(\theta) = q_0$.
4. $\phi_1(\theta) = \phi_2(\theta) = 0$, $q_1(\theta) = 0$, $q_2(\theta) = q_0 H(\beta/2 - |\theta - \alpha/2|)$, $\beta/\alpha = 0.1$

where $H(\theta)$ is Heavyside's unit step function. The results for various cases can be superposed as the governing equations are linear. The results for cases of $q_0 \neq 0$ and $\phi_0 \neq 0$ are, respectively, expressed in dimensionless form as follows:

$$\bar{u} = 100 Y_r u/hs^4 q_0, \quad \bar{\sigma}_r = \sigma_r/q_0, \quad \bar{\sigma}_z = \sigma_z/s^2 q_0, \quad \bar{\phi} = |d_1| Y_r \phi/hs^2 q_0$$
$$\bar{v} = 100 Y_r v/hs^4 q_0, \quad \bar{\sigma}_\theta = \sigma_\theta/s^2 q_0, \quad \bar{\tau}_{r\theta} = \tau_{r\theta}/sq_0, \quad (\bar{D}_r, \bar{D}_\theta) = (D_r, D_\theta)/|d_1| sq_0; \quad (46)$$

$$\tilde{u} = 100u/|d_1| s\phi_0, \quad \tilde{\sigma}_r = s^3 h\sigma_r/Y_r|d_1|\phi_0, \quad \tilde{\sigma}_z = h\sigma_z/Y_r|d_1|\phi_0,$$
$$\tilde{\phi} = \phi/\phi_0, \quad \tilde{v} = 100v/|d_1| s\phi_0, \quad \tilde{\sigma}_\theta = s^2 h\sigma_\theta/Y_r|d_1|\phi_0,$$
$$\tilde{\tau}_{r\theta} = s^3 h\tau_{r\theta}/Y_r|d_1|\phi_0, \quad (\tilde{D}_r, \tilde{D}_\theta) = h(D_r, sD_\theta)/d_1^2 Y_r \phi_0. \quad (47)$$

The results are presented in tabular form to facilitate quantitative assessment of the accuracy of other approximate methods of solution as well as the accuracy of the two dimensional plate theory formulations. Results have been obtained for eight values of the radius (of the middle surface) to thickness ratio $s = R/h = 2, 4, 6, 10, 20, 50, 100, 500$.

The following two problems are solved to check the validity of the programme developed for numerical computation. Consider a simply-supported circular cylindrical panel with $\alpha = 60°$, subjected to a sinusoidal mechanical load of case 1 with the following mechanical properties:

$$Y_r : Y_\theta : Y_z : G_{r\theta} : G_{\theta z} : G_{zr} = 1 : 25 : 1 : 0.5 : 0.5 : 0.2, \quad \nu_{\theta r} = \nu_{\theta z} = \nu_{rz} = 0.25,$$
$$e_1 = e_3 = 10^{-10}\ \mathrm{Cm}^{-2}, \quad e_2 = e_6 = 0, \quad \eta_i = 10^{-10}\ \mathrm{C}^2\ \mathrm{N}^{-1}\ \mathrm{m}^{-2}.$$

The coupling between the elastic and electric fields is very weak since e_i are very small. The results of the present exact solution for the case of weakly coupled piezoelectric material are compared in Table 1 with the results of the exact uncoupled elasticity solution presented by Ren (1987). The values of all the entities obtained by the two different formulations are in excellent agreement for both thick and thin cylindrical panels with $s = 2$ and 100.

Consider an almost flat simply-supported cylindrical panel with $R/h = 1000$, $R = 1$ m such that its span l to thickness h ratio $l/h = ls/R = \alpha s = 2$. It is subjected to the following electromechanical loads: $\phi_1(\theta) = \phi_0 \sin(\pi\theta/\alpha)$, $\phi_2(\theta) = 0$, $q_1(\theta) = 0$, $q_2(\theta) = q_0 \sin(\pi\theta/\alpha)$ with $q_0 = -10\ \mathrm{N/m^2}$ and $\phi_0 = 0$ or 200 V. The material is taken to be isotropic with Youngs modulus $Y = 2$ GPa, Poisson's ratio $\nu = 0.25$, $e_1 = e_6 = 0$, $e_2 = e_3 = 0.046$ C m^{-2} and $\eta_i = 0.1062 \times 10^{-9}\ \mathrm{C^2\ N^{-1}\ m^{-2}}$. The present exact solution of such a piezoelectric cylindrical shell panel is compared in Table 2 with the exact solution presented by Ray *et al.* (1992) for simply-supported flat piezoelectrical panel. The values listed have been read off from the figures in their paper. There is very good agreement between the numerical values of various entities obtained by two different procedures. It may be noted that the exact formulation for shell panel involves Euler–Cauchy type of differential equations with variable coefficients, whereas the exact formulation given by Ray *et al.* (1992) for flat panels involves differential equations with constant coefficients. Thus the analytical functional form of the two solutions is quite different.

Table 1. Comparison of piezoelastic solution with elastic solution

R/h	2 Present	2 Ren (1987)	500 Present	500 Ren (1987)
$\bar{u}(\alpha/2, 0)$	9.976	9.986	0.7490	0.749
$\bar{\sigma}_\theta(\alpha/2, -h/2)$	−2.455	−2.455	−0.7515	−0.752
$\bar{\sigma}_\theta(\alpha/2, h/2)$	1.907	1.907	0.7500	0.750
$\bar{\sigma}_z(\alpha/2, -h/2)$	−0.02455	−0.0245	−0.007515	−0.0075
$\bar{\sigma}_z(\alpha/2, h/2)$	0.08157	0.0816	0.007501	0.0075
$\bar{\tau}_{r\theta}(0, 0)$	0.5553	0.555	0.5631	0.563

Table 2. Comparison of piezoelastic solution for an almost flat cylindrical panel with the solution for a flat panel

ϕ_1	0 Present	0 Ray (1992)	200 Present	200 Ray (1992)
$100Y_r h^3(\alpha/2, h/2)/q_0 l^4$	19.308	19.3	−2830.4	−2820
$Y_r v(0, -h/2)/hq_0$	1.5181	1.50	−789.89	−790
$\sigma_\theta(\alpha/2, -h/2)/q_0$	−2.5608	−2.54	−249.41	−250
$\sigma_r(\alpha/2, 0)/q_0$	0.49280	0.5	16.646	16.5
$\tau_{r\theta}(0, 0)/q_0$	0.93414	0.92	—	—
$\tau_{r\theta}(0, 0.3h)/q_0$	—	—	−29.896	−30
$\phi(\alpha/2, 0)$	—	—	75.653	75.5
$10^3 D_r(\alpha/2, h/2)/e_2$	—	—	0.31895	0.315

Table 3. Convergence study

N	$\bar{u}(\alpha/2, h/2)$	$\bar{v}(0, h/2)$	$\bar{\sigma}_\theta(\alpha/2, h/2)$
49	−4.3052	−0.19621	−0.20906
99	−4.3060	−0.19627	−0.21219
199	−4.3055	−0.19627	−0.20838
299	−4.3056	−0.19627	−0.21050
399	−4.3055	−0.19627	−0.20901
499	−4.3056	−0.19627	−0.21016

Table 4. Effect of radius to thickness ratio s for case 1

R/h	2	4	6	10	20	100	500
$\bar{u}(\alpha/2, -h/2)$	−28.65	−20.55	−18.72	−17.60	−16.96	−16.55	−16.48
$\bar{u}(\alpha/2, 0)$	−31.47	−21.10	−18.96	−17.68	−16.98	−16.55	−16.48
$\bar{u}(\alpha/2, h/2)$	−31.31	−20.65	−18.73	−17.60	−16.95	−16.55	−16.48
$\bar{v}(0, -h/2)$	−23.61	−13.09	−10.23	−8.177	−6.778	−5.738	−5.539
$\bar{v}(0, h/2)$	2.046	−0.8806	−2.331	−3.572	−4.528	−5.297	−5.451
$\bar{\sigma}_r(\alpha/2, 0)$	−0.2906	0.2170	0.6356	1.420	3.319	18.34	93.34
$\bar{\sigma}_\theta(\alpha/2, -h/2)$	1.276	0.9735	0.8904	0.8304	0.7888	0.7576	0.7515
$\bar{\sigma}_\theta(\alpha/2, h/2)$	−0.8057	−0.7597	−0.7540	−0.7514	−0.7503	−0.7500	−0.7500
$\bar{\sigma}_z(\alpha/2, -h/2)$	0.4265	0.3257	0.2980	0.2779	0.2640	0.2535	0.2515
$\bar{\sigma}_z(\alpha/2, h/2)$	−0.3527	−0.2750	−0.2615	−0.2548	−0.2519	−0.2510	−0.2510
$\bar{\tau}_{r\theta}(0, 0)$	−0.6653	−0.6238	−0.6055	−0.5893	−0.5762	−0.5653	−0.5631
$10^3\bar{\phi}(\alpha/2, 0)$	1.734	2.443	2.541	2.560	2.540	2.504	2.494
$10\bar{D}_r(\alpha/2, -h/2)$	5.908	2.550	1.532	0.7830	0.2659	−0.1171	−0.1902
$10\bar{D}_r(\alpha/2, h/2)$	0.8480	0.0213	−0.0996	−0.1575	−0.1860	−0.2041	−0.2075
$\bar{D}_\theta(0, 0)$	−0.3070	−0.4324	−0.4497	−0.4531	−0.4496	−0.4431	−0.4415

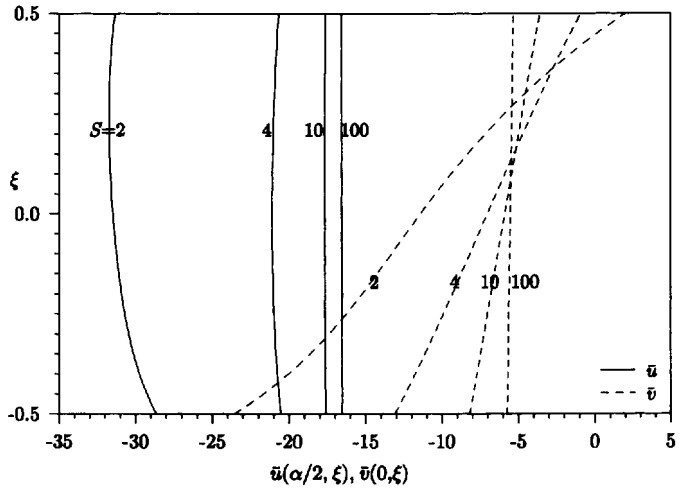

Fig. 2. Distributions of $\bar{u}$ and $\bar{v}$ across the thickness for case 1.

Computations have been carried out for a cylindrical shell panel with $\alpha = 60^\circ$ made out of PVDF polarised perpendicular to its curved surface, i.e., in the radial direction. Its material parameters are assumed as

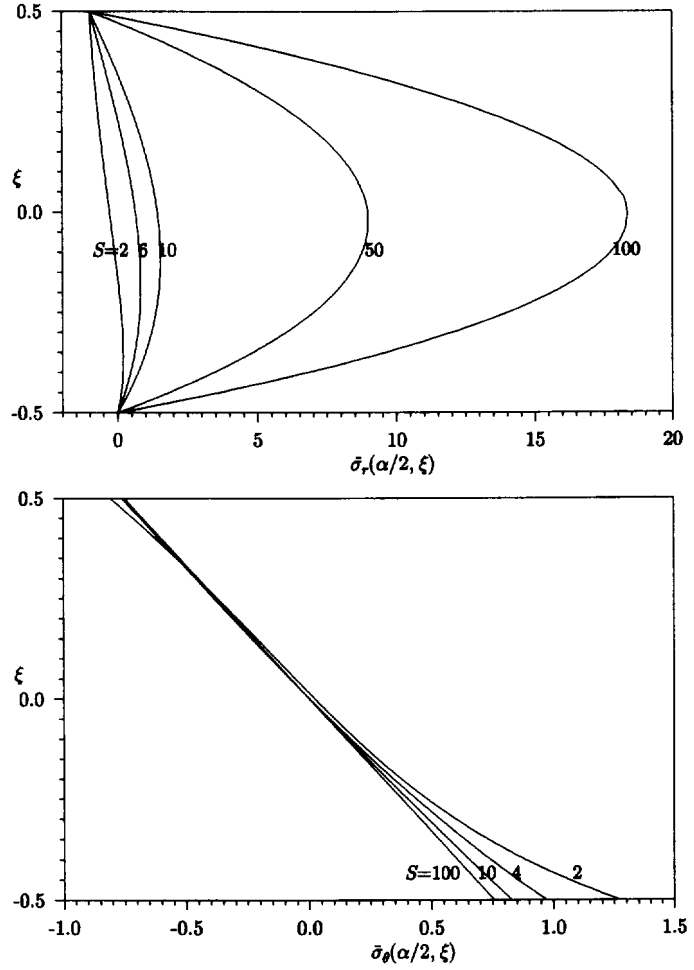

Fig. 3. Distributions of $\bar{\sigma}_r$ and $\bar{\sigma}_\theta$ across the thickness for case 1.

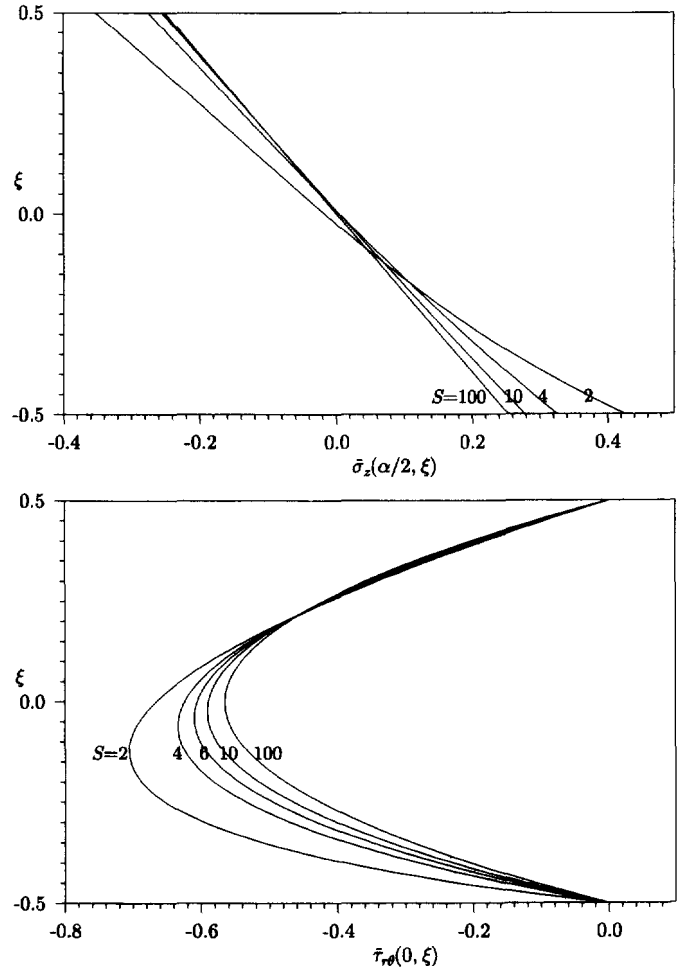

Fig. 4. Distributions of $\bar{\sigma}_z$ and $\bar{\tau}_{r\theta}$ across the thickness for case 1.

$$d_1 = -30 \times 10^{-12}\,\mathrm{C\,N^{-1}}, \quad e_1 = -0.051\,\mathrm{C\,m^{-2}}, \quad Y = 2\,\mathrm{GPa}, \quad \nu = 1/3,$$

$$\eta_i = 106.2 \times 10^{-12}\,\mathrm{C^2\,N^{-1}\,m^{-2}}, \quad e_2 = 0.0285\,\mathrm{C\,m^{-2}}, \quad e_3 = -0.0015\,\mathrm{C\,m^{-2}}, \quad e_6 = 0.$$

The constants e_i correspond to piezoelectric coefficients $d_{ri} = (-30, 23, 3) \times 10^{-12}\,\mathrm{N^{-1}}$. Only one term solution is needed for sinusoidal loading. Convergence studies have been conducted for non-sinusoidal loadings. The results of a typical convergence study are presented in Table 3 for a panel with $s = 4$ subjected to loading of case 5, i.e., its curved surfaces are held at zero potential and the outer surface is subjected to uniform pressure for the middle one-tenth of the span. It is observed that accurate results are obtained even for $N = 49$. The bending stress σ_θ for points on the lateral surface is the slowest to converge. All results presented in this study for non-sinusoidal loadings, symmetric about $\theta = \alpha/2$, have been obtained with $N = 499$, i.e., with 250 non-zero odd terms.

Results of various entities at locations where they are high are presented in Table 4 for case 1 of sinusoidal pressure loading on the outer surface of the panel with its both lateral surfaces held at zero potential. The variation across the thickness $[\xi = (r - R)/h]$ of the displacements $\bar{u}$ at $\theta = \alpha/2$ and $\bar{v}$ at $\theta = 0$ is depicted in Fig. 2 for five values of s. Similar variations across the thickness of $\bar{\sigma}_r$ and $\bar{\sigma}_\theta$ at $\theta = \alpha/2$ are shown in Fig. 3. The distributions across the thickness of $\bar{\sigma}_z$ at $\theta = \alpha/2$ and $\bar{\tau}_{r\theta}$ at $\theta = 0$ are depicted in Fig. 4. The distributions of $\bar{\phi}$ and $\bar{D}_r$ at $\theta = \alpha/2$ are shown in Fig. 5. It is observed that, for $s \geqslant 4$, $\bar{u}$ is almost uniform across the thickness and $\bar{v}$ varies almost linearly across the thickness. The variation of $\bar{\sigma}_r$, $\bar{\tau}_{r\theta}$ and $\bar{\phi}$ across the thickness is almost quadratic. The variation of the bending stress $\bar{\sigma}_\theta$ and axial stress $\bar{\sigma}_z$ across the thickness is quite nonlinear for $s \leqslant 10$. The distribution of

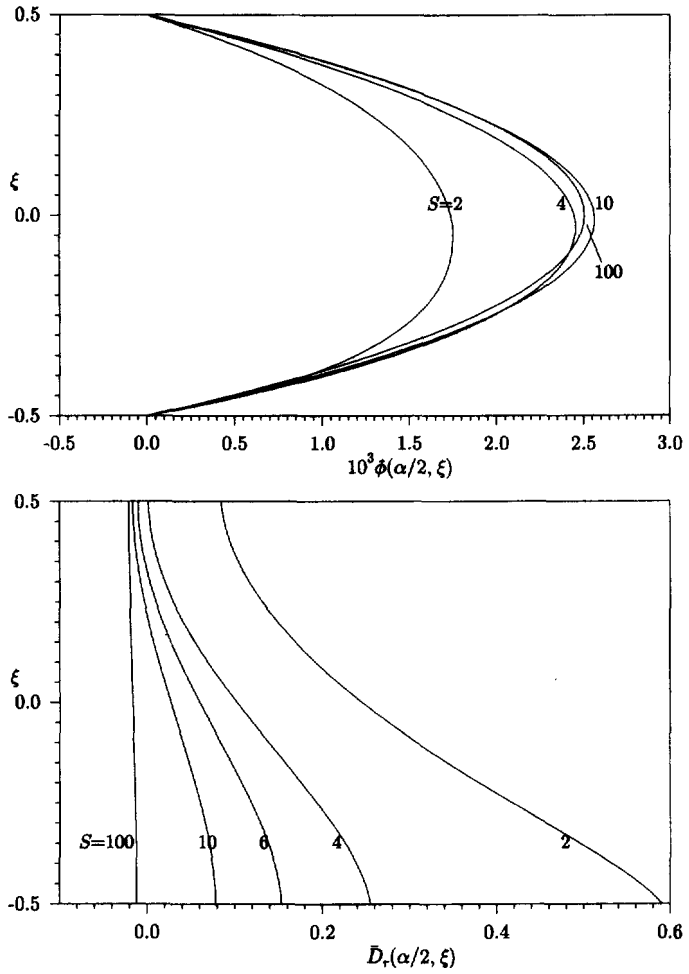

Fig. 5. Distributions of $\bar{\phi}$ and $\bar{D}_r$ across the thickness for case 1.

Table 5. Effect of radius to thickness ratio s for case 2

R/h	2	4	6	10	20	100	500
$\tilde{u}(\alpha/2, -h/2)$	39.37	23.94	17.11	11.24	6.694	3.008	2.268
$\tilde{u}(\alpha/2, 0)$	17.96	11.90	8.955	6.340	4.253	2.523	2.171
$\tilde{u}(\alpha/2, h/2)$	−8.480	−0.2131	0.9961	1.575	1.860	2.041	2.075
$\tilde{v}(0, -h/2)$	3.359	−13.78	−18.72	−22.10	−24.23	−25.66	−25.91
$\tilde{v}(0, h/2)$	−35.98	−28.74	−27.27	−26.49	−26.13	−25.99	−25.98
$\tilde{\sigma}_\theta(\alpha/2, -h/2)$	−1.544	−1.536	−1.505	−1.410	−1.439	−1.411	−1.405
$\tilde{\sigma}_\theta(\alpha/2, 0)$	0.5990	0.6768	0.6920	0.6995	0.7020	0.7019	0.7017
$\tilde{\sigma}_\theta(\alpha/2, h/2)$	−1.141	−1.266	−1.309	−1.345	−1.373	−1.397	−1.402
$\tilde{\sigma}_z(\alpha/2, -h/2)$	−0.2204	−0.1359	−0.1185	−0.1086	−0.1034	−0.1005	−0.1001
$\tilde{\sigma}_z(\alpha/2, h/2)$	−0.2262	−0.1307	−0.1117	−0.1024	−0.0994	−0.0996	−0.0999
$\tilde{\tau}_{r\theta}(0, -h/4)$	0.3538	0.3925	0.3975	0.3984	0.3973	0.3953	0.3948
$\bar{\phi}(\alpha/2, 0)$	−0.4433	−0.4978	−0.5057	−0.5070	−0.5049	−0.5012	−0.5002
$\bar{D}_r(\alpha/2, -h/2)$	54.91	62.48	62.91	62.39	61.51	60.49	60.26
$\bar{D}_r(\alpha/2, h/2)$	78.73	62.77	59.92	58.96	59.15	59.92	60.14
$\bar{D}_\theta(0, h/2)$	141.6	157.3	163.4	168.6	172.7	176.1	176.8

electrical displacement $\bar{D}_r$ across the thickness is nonlinear which tends to a uniform distribution for $s \geqslant 500$.

The dimensionless results for case 2 of sinusoidal electric potential distribution applied to the outer surface of the panel with no pressure loading are presented in Table 5. The through-the-thickness variations of transverse displacement $\tilde{u}$ at the middle and inplane

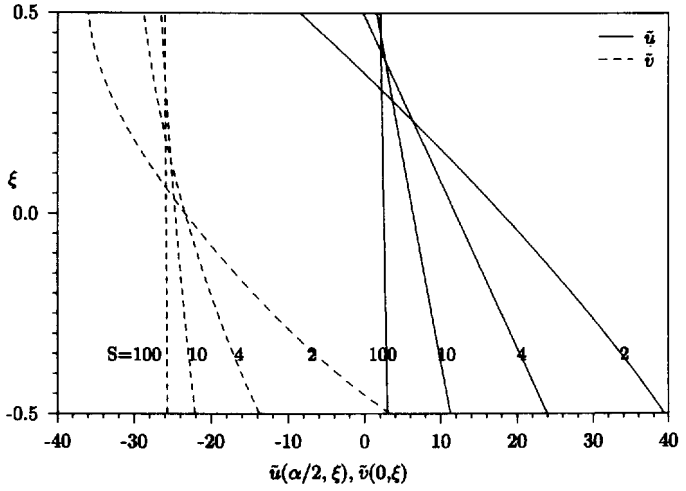

Fig. 6. Distributions of $\tilde{u}$ and $\tilde{v}$ across the thickness for case 2.

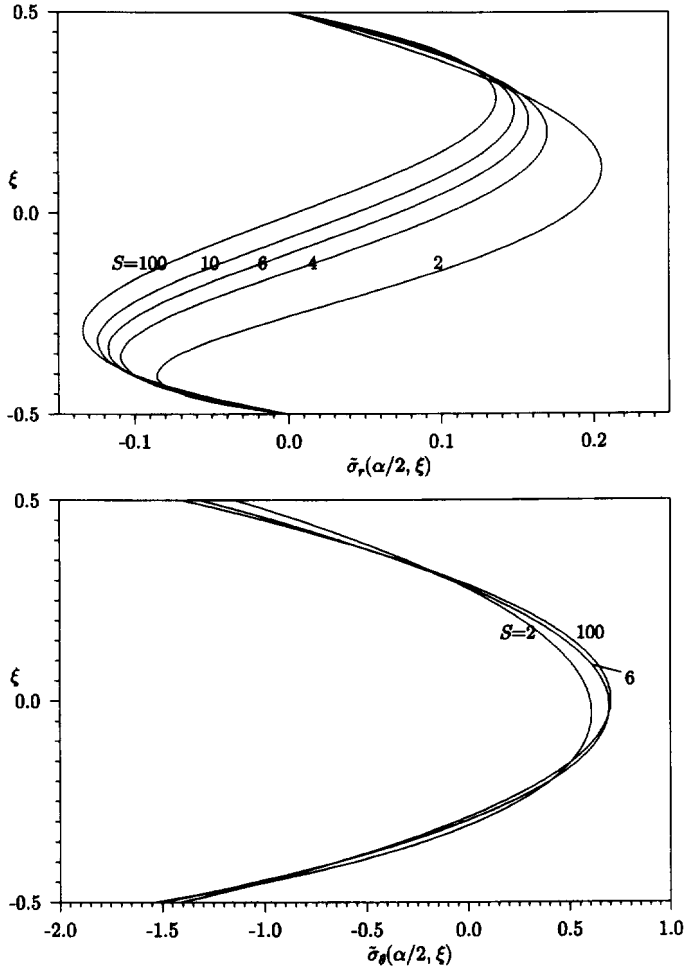

Fig. 7. Distributions of $\tilde{\sigma}_r$ and $\tilde{\sigma}_\theta$ across the thickness for case 2.

displacement $\tilde{v}$ at the end are shown in Fig. 6. Similar distributions of the stress components $\tilde{\sigma}_r$, $\tilde{\sigma}_\theta$ and $\tilde{\sigma}_z$, $\tilde{\tau}_{r\theta}$ are presented in Figs 7 and 8. The distributions of electrical potential $\tilde{\phi}$ and electrical displacement $\tilde{D}_r$ are plotted in Fig. 9. The distributions of displacements $\tilde{u}$ and $\tilde{v}$ across the thickness are almost uniform for $s = 100$. Their distributions first become linear and then nonlinear as s decreases for thicker shells. The distributions of $\tilde{\sigma}_r$ and $\tilde{\tau}_{r\theta}$ are S-shaped. The distributions of bending stress $\tilde{\sigma}_\theta$ and the axial stress $\tilde{\sigma}_z$ are almost

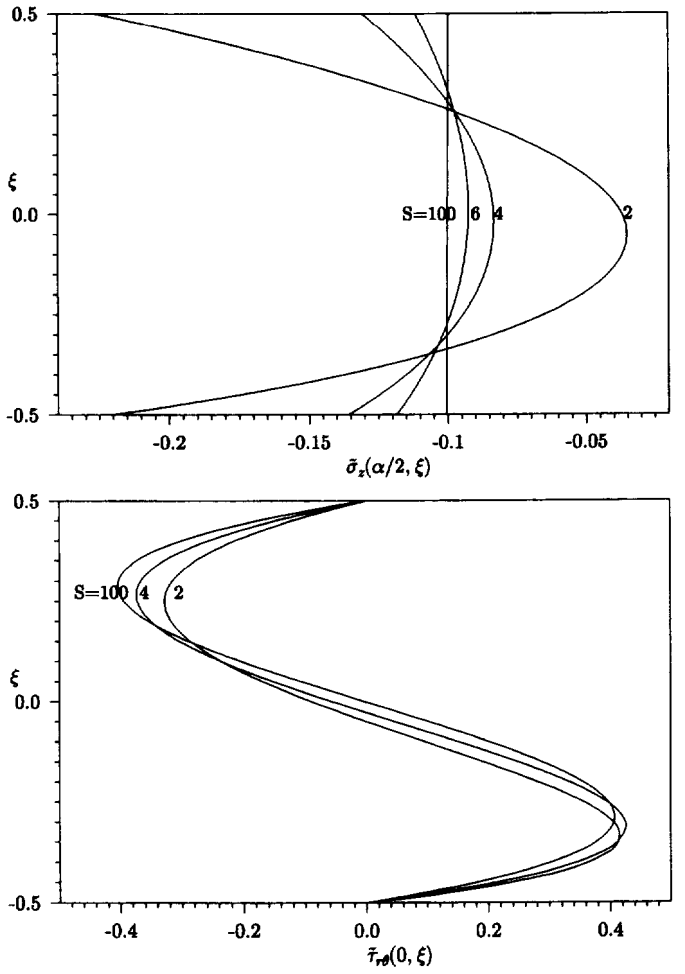

Fig. 8. Distributions of $\tilde{\sigma}_z$ and $\tilde{\tau}_{r\theta}$ across the thickness for case 2.

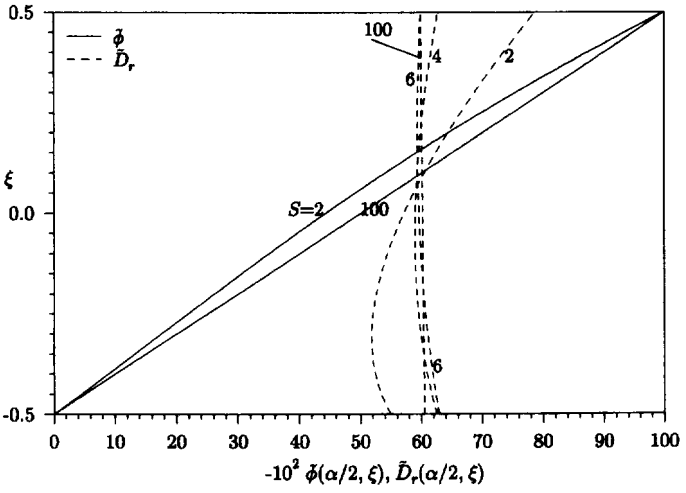

Fig. 9. Distributions of $\tilde{\phi}$ and $\tilde{D}_r$ across the thickness for case 2.

quadratic across the thickness. The distribution of the electric potential $\tilde{\phi}$ across the thickness tends to a linear one for $s \geqslant 10$. The distribution of the electrical displacement $\tilde{D}_r$ across the thickness tends towards a uniform one for $s \geqslant 10$.

The results of cases 1 and 2 are superposed to obtain the solution for the case of simultaneous application of sinusoidal pressure $q_2(\theta) = q_0 \sin(\pi\theta/\alpha)$ and electric potential $\phi_2(\theta) = -\phi_0 \sin(\pi\theta/\alpha)$ on a cylindrical panel with $s = 10$. The distributions of the deflection

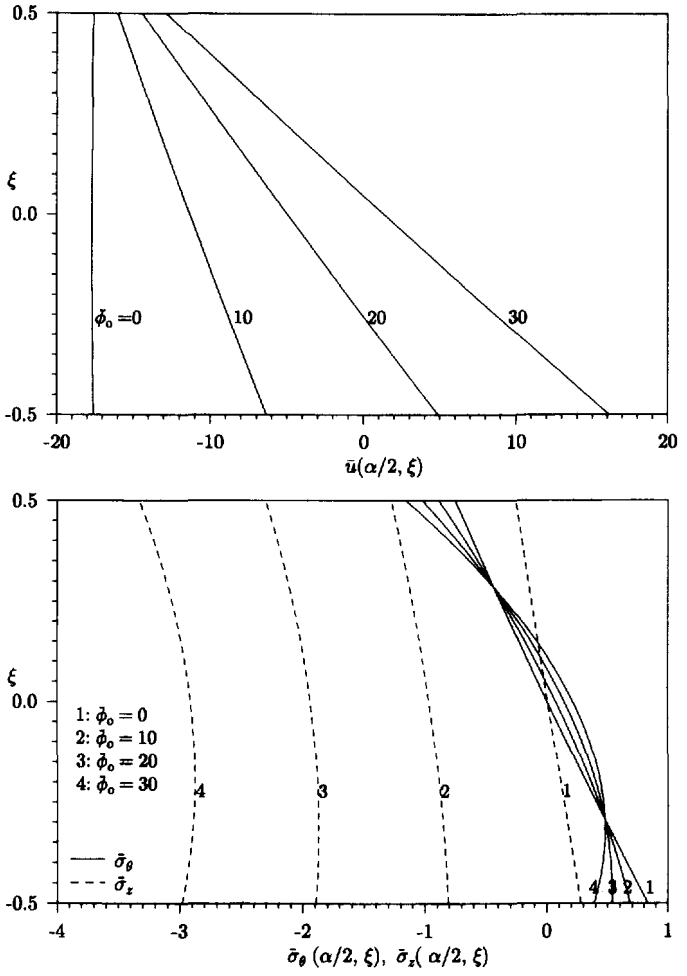

Fig. 10. Distributions of $\bar{u}$, $\bar{\sigma}_\theta$ and $\bar{\sigma}_z$ for combined loadings of cases 1 and 2.

Table 6. Effect of radius to thickness ratio s for case 3

R/h	2	4	6	10	20	100	500
$\bar{u}(\alpha/2, -h/2)$	−36.32	−26.04	−23.74	−22.33	−21.52	−21.01	−20.92
$\bar{u}(\alpha/2, 0)$	−39.65	−26.71	−24.03	−22.43	−21.54	−21.01	−20.92
$\bar{u}(\alpha/2, h/2)$	−38.87	−26.11	−23.74	−22.33	−21.52	−21.01	−20.92
$\bar{v}(0, -h/2)$	−30.21	−16.79	−13.10	−10.46	−8.657	−7.318	−7.061
$\bar{v}(0, h/2)$	3.095	−1.029	−2.916	−4.521	−5.755	−6.749	−6.947
$\bar{\sigma}_r(\alpha/2, 0)$	−0.2193	0.4149	0.9237	1.887	4.232	22.82	115.6
$\bar{\sigma}_\theta(\alpha/2, -h/2)$	1.591	1.203	1.101	1.027	0.9761	0.9375	0.9301
$\bar{\sigma}_\theta(\alpha/2, h/2)$	−0.9545	−0.9349	−0.9312	−0.9293	−0.9285	−0.9282	−0.9282
$\bar{\sigma}_z(\alpha/2, -h/2)$	0.5320	0.4024	0.3683	0.3437	0.3267	0.3138	0.3113
$\bar{\sigma}_z(\alpha/2, h/2)$	−0.4021	−0.3335	−0.3208	−0.3143	−0.3116	−0.3107	−0.3106
$\bar{\tau}_{r\theta}(0, 0)$	−0.9501	−0.9178	−0.9029	−0.8892	−0.8781	−0.8682	−0.8653
$10^3\bar{\phi}(\alpha/2, 0)$	2.260	3.080	3.174	3.179	3.146	3.099	3.087
$10\bar{D}_r(\alpha/2, -h/2)$	6.892	2.665	1.538	0.7496	0.2210	−0.1659	−0.2396
$10\bar{D}_r(\alpha/2, h/2)$	0.3913	−0.1691	−0.2058	−0.2279	−0.2431	−0.2549	−0.2572
$\bar{D}_\theta(0, 0)$	−0.3198	−0.5334	−0.5900	−0.6295	−0.6557	−0.6750	−0.6780

$\bar{u}$, bending stress $\bar{\sigma}_\theta$ and axial stress $\bar{\sigma}_z$ across the thickness at $\theta = \alpha/2$ are depicted in Fig. 10 for four values of $\bar{\phi}_0$. It is observed from the numerical results that the midsurface transverse displacement under pressure loading can be reduced by appropriate application of electrical potential difference between the inner and outer surfaces of the shell panel.

Table 7. Effect of radius to thickness ratio s for case 4

R/h	2	4	6	10	20	100	500
$\bar{u}(\alpha/2, -h/2)$	−5.782	−4.166	−3.788	−3.553	−3.417	−3.334	−3.320
$\bar{u}(\alpha/2, 0)$	−6.536	−4.311	−3.847	−3.572	−3.422	−3.334	−3.320
$\bar{u}(\alpha/2, h/2)$	−7.661	−4.306	−3.816	−3.556	−3.417	−3.334	−3.320
$\bar{v}(0, -h/2)$	−4.638	−2.565	−2.009	−1.612	−1.340	−1.138	−1.100
$\bar{v}(0, h/2)$	0.3552	−0.1963	−0.4789	−0.7197	−0.9044	−1.053	−1.083
$\bar{\sigma}_r(\alpha/2, 0)$	−0.1902	−0.2302	−0.2255	−0.1085	0.3538	3.844	21.15
$\bar{\sigma}_\theta(\alpha/2, -h/2)$	0.2710	0.2205	0.2049	0.1923	0.1824	0.1748	0.1734
$\bar{\sigma}_\theta(\alpha/2, h/2)$	−0.3645	−0.2102	−0.1860	−0.1762	−0.1736	−0.1731	−0.1731
$\bar{\sigma}_z(\alpha/2, -h/2)$	0.0906	0.0737	0.0686	0.0644	0.0611	0.0585	0.0580
$\bar{\sigma}_z(\alpha/2, h/2)$	−0.2058	−0.0913	−0.0716	−0.0623	−0.0589	−0.0580	−0.0579
$\bar{\tau}_{r\theta}(0, 0)$	−0.1074	−0.1009	−0.0978	−0.0950	−0.0929	−0.0911	−0.0907
$10^3\bar{\phi}(\alpha/2, 0)$	0.2882	0.4790	0.5292	0.5619	0.5773	0.5774	0.5755
$10\bar{D}_r(\alpha/2, -h/2)$	1.526	1.122	0.9564	0.7349	0.4034	0.0410	−0.0303
$10\bar{D}_r(\alpha/2, h/2)$	2.267	0.9558	0.5293	0.2051	0.0146	−0.0396	−0.0464
$\bar{D}_\theta(0, 0)$	−0.0687	−0.0781	−0.0764	−0.0744	−0.0728	−0.0714	−0.0711

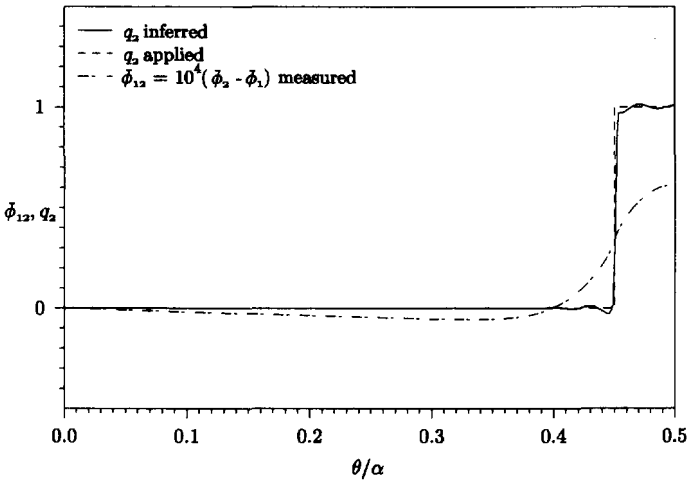

Fig. 11. Distributions of measured potential difference, inferred q_2 and applied q_2 for inverse problem.

However, it results in a significant increase in the normal stress in the longitudinal direction. The transverse displacement $\bar{u}$ of the middle surface is significantly reduced for $\bar{\phi}_0 = 30$.

The results for case 3 of a circular cylindrical panel with its lateral surfaces held at zero potential and its outer surface subjected to uniform pressure q_0 are presented in Table 6. The results for case 4 of a cylindrical panel with its lateral surfaces held at zero potential and its outer surface subjected to uniform pressure on the middle one-tenth of the span are presented in Table 7. Comparison of the results of case 1 of sinusoidal pressure loading with the results of cases 3 and 4 of uniform and patch pressure loadings has revealed that the various entities have qualitatively similar through-the-thickness distributions for these three cases.

In order to illustrate the validity of the solution procedure for the inverse problem even for an extreme condition of pressure loading, we consider a cylindrical panel with its lateral surfaces charge free, i.e., $D_1(\theta) = D_2(\theta) = 0$, the internal surface traction free and the external surface subjected to a pressure profile of a rectangular patch in the middle one-tenth of the span as in case 4 above. The solution of the direct problem for a simply-supported panel with $s = 10$ yields the potential difference $V(x)$ between the two curved surfaces of the panel. In the inverse problem, this potential difference distribution, shown in Fig. 11, is taken as the known potential difference distribution for a panel with charge free surfaces. The inferred profile of the pressure q_2 is compared in Fig. 11 with the applied

pressure profile. There is very good agreement between the inferred and the applied profiles even for this extreme case.

7. CONCLUSIONS

Exact analytical solutions have been presented for the direct and inverse piezoelastic problems of infinitely long, simply-supported, cylindrically orthotropic circular cylindrical panel in cylindrical bending under pressure and electrostatic excitation. Detailed results have been presented for sinusoidal, uniform and patch loadings. As in the case of elastic shell panels, the piezoelastic shell panels subjected to pressure loading experience tensile normal stress in the radial direction. Numerical results have revealed that the midsurface transverse displacement under pressure loading can be reduced by appropriate application of electrical potential difference between the inner and outer surfaces of the shell panel. However, it results in a significant increase in the normal stress in the longitudinal direction. The solution of the inverse problem has established that the applied pressure profile can be inferred from the measured potential difference between the lateral surfaces of the shell panel. The numerical results presented for the exact analytical series solution would help in validating approximate solutions obtained by other methods. The exact distributions of several entities across the thickness are presented in this study for various cases of electro-mechanical loads on cylindrical panels with the ratio of mean radius to thickness varying from 2 to 100. These would help in the validation of two-dimensional theories for piezo-elastic thin and thick shells as well as for shallow and deep shells. The formulation is being extended to obtain exact solution of laminated simply-supported cylindrical panels with piezoelectric layers.

REFERENCES

Crawley, F. E. (1994). Intelligent structures for aerospace: a technology overview and assessment. *AIAA J.* **32,** 1689–1700.

Heyliger, P. (1994). Static behavior of laminated elastic/piezoelectric plates. *AIAA J.* **32,** 2481–2484.

Mitchell, J. A. and Reddy, J. N. (1995). A study of embedded piezoelectric layers in composite cylinders. *J. Appl. Mech.* **62,** 166–173.

Ray, M. C., Rao, K. M. and Samanta, B. (1992). Exact analysis of coupled electroelastic behavior of a piezoelectric plate under cylindrical bending. *Comput. Struct.* **45,** 667–677.

Ray, M. C., Rao, K. M. and Samanta, B. (1993a). Exact solution of an intelligent structure under cylindrical bending. *Comput. Struct.* **47,** 1031–1042.

Ray, M. C., Rao, K. M. and Samanta, B. (1993b). Exact solutions for static analysis of intelligent structures. *AIAA J.* **31,** 1684–1691.

Ren, J. G. (1987). Exact solutions for laminated cylindrical shells in cylindrical bending. *Comp. Sci. Tech.* **29,** 169–187.

Smirnov, V. I. (1964). *A Course of Higher Mathematics*, Vol. 1, pp. 491–497, Pergamon Press, London.

Tiersten, H. F. (1969). *Piezoelectric Plate Vibration*, pp. 54–55, Plenum Press, New York.